

2011

Tuning the Thermal Relaxation of Transition-Metal Ferrite Nanoparticles Through Their Intrinsic Magnetocrystalline Anisotropy

Jose M. Vargas
University of New Orleans, jmvargas@uno.edu

Abhishek Srivastava
University of New Orleans, abhi.alld@gmail.com

Amin Yourdkhani
University of New Orleans, ayourdkh@uno.edu

Luis Zaldivar
University of New Orleans, lzadliva@uno.edu

Gabriel Caruntu
University of New Orleans, gcaruntu@uno.edu

See next page for additional authors

Follow this and additional works at: https://scholarworks.uno.edu/chem_facpubs

 Part of the [Chemistry Commons](#)

Recommended Citation

J. Appl. Phys. 110, 064304 (2011);

This Article is brought to you for free and open access by the Department of Chemistry at ScholarWorks@UNO. It has been accepted for inclusion in Chemistry Faculty Publications by an authorized administrator of ScholarWorks@UNO. For more information, please contact scholarworks@uno.edu.

Authors

Jose M. Vargas, Abhishek Srivastava, Amin Yourdkhani, Luis Zaldivar, Gabriel Caruntu, and Leonard Spinu

Tuning the thermal relaxation of transition-metal ferrite nanoparticles through their intrinsic magnetocrystalline anisotropy

José M. Vargas, Abhishek Srivastava, Amin Yourdkhani, Luis Zaldivar, Gabriel Caruntu et al.

Citation: *J. Appl. Phys.* **110**, 064304 (2011); doi: 10.1063/1.3638053

View online: <http://dx.doi.org/10.1063/1.3638053>

View Table of Contents: <http://jap.aip.org/resource/1/JAPIAU/v110/i6>

Published by the [American Institute of Physics](#).

Related Articles

Peculiarly strong room-temperature ferromagnetism from low Mn-doping in ZnO grown by molecular beam epitaxy

AIP Advances **3**, 032110 (2013)

In-plane anisotropic converse magnetoelectric coupling effect in FeGa/polyvinylidene fluoride heterostructure films

J. Appl. Phys. **113**, 17C705 (2013)

First principles study of magnetic anisotropy and magnetoelectric effect of FePd/MgO(001) ultrathin films

J. Appl. Phys. **113**, 17C702 (2013)

Electric-voltage control of magnetism in Fe/BaTiO₃ heterostructured multiferroics

J. Appl. Phys. **113**, 17C701 (2013)

Reducing the writing field of L10-FePt by graded order parameter

J. Appl. Phys. **113**, 073912 (2013)

Additional information on *J. Appl. Phys.*

Journal Homepage: <http://jap.aip.org/>

Journal Information: http://jap.aip.org/about/about_the_journal

Top downloads: http://jap.aip.org/features/most_downloaded

Information for Authors: <http://jap.aip.org/authors>

ADVERTISEMENT



AIP Advances

Now Indexed in
Thomson Reuters
Databases

Explore AIP's open access journal:

- Rapid publication
- Article-level metrics
- Post-publication rating and commenting

Tuning the thermal relaxation of transition-metal ferrite nanoparticles through their intrinsic magnetocrystalline anisotropy

José M. Vargas, Abhishek Srivastava, Amin Yourdkhani, Luis Zaldivar, Gabriel Caruntu, and Leonard Spinu^{a)}

Advanced Materials Research Institute, University of New Orleans, New Orleans, Louisiana 70148, USA

(Received 6 May 2011; accepted 5 August 2011; published online 19 September 2011)

Monodispersed ferrite nanoparticles of Fe_3O_4 , MnFe_2O_4 , and CoFe_2O_4 (near to 10 nm), were synthesized by organometallic synthesis, showing the same homogeneous chemical, morphological, and crystalline characteristics. The study and correlation of the thermal relaxation processes were analyzed through static and dynamic measurements. Due to the intrinsic chemical characteristics and magnetocrystalline anisotropy of the ferrite nanoparticles, the energy barrier can be tuned to a range between $1100 \text{ K} \leq E_B \leq 7300 \text{ K}$, showing an alternative approach for tuning the magnetic dynamic properties, in contrast to the well-known mechanism through particle-size-effects. Specific loss power efficiencies were evaluated for the three ferrite samples. Comparing the three samples at the maximum *ac* frequency of $\nu = 10 \text{ kHz}$, MnFe_2O_4 exhibits the single-peak maximum of loss with the value of $273 \text{ erg/s} \cdot \text{g}$ at $T = 65 \text{ K}$, whereas for the CoFe_2O_4 , a maximum of $132 \text{ erg/s} \cdot \text{g}$ ($T = 217 \text{ K}$) was determined. A considerable drop in the efficiency was determined for the Fe_3O_4 nanoparticles, with the value of $20 \text{ erg/s} \cdot \text{g}$ at $T = 43.5 \text{ K}$. © 2011 American Institute of Physics. [doi:10.1063/1.3638053]

I. INTRODUCTION

Over the last five decades, much work has been devoted to study the dynamic properties of small particles, from theoretical as well as experimental perspectives.^{1,2} Below a critical diameter, the particles become single domain and have interesting properties such as superparamagnetism and strong surface effects.³ These properties depend on the size and shape of particles, on the interaction between them, and on the effects of finite size and superparamagnetic relaxation.⁴⁻⁶ The magnetic properties of nanoparticles are determined by many factors, the key of which are the chemical composition, the type, and the degree of defectiveness of the crystal lattice, the particle size and shape, the morphology, and the interaction of the particle with the surrounding matrix and the neighboring particles. By changing the nanoparticle size, shape, composition, and structure, one can control the magnetic properties of the material based on them.⁷ Magnetic transition-metal nanoparticles (NPs) are used in a number of applications including ferrofluids, biosensors, contrast enhancement agents for magnetic resonance imaging, bioprobes, and catalysis.⁸⁻¹⁰ Magnetic hyperthermia for tumor treatment has attracted much attention due to the considerable heating effect in an *ac* magnetic field. Briefly, the heating effect of magnetic fluid results from the absorption of energy from *ac* magnetic field and conversion into heat by eddy current losses and relaxation losses. For example, Hergt *et al.*¹¹ studied the validity limits of the Néel relaxation model of magnetic NPs for hyperthermia, where based on their phenomenological model, the specific loss power (SLP) was discussed as a function of the particle size and magnetic field amplitude in the whole size range from superparamagnetic

up to multidomain particles including the effect of size distribution were discussed. Regarding to this application, the enhancement of the SLP is required with the following restrains: (i) using particles with a mean size near to 10 nm and (ii) at the physiologically tolerable range of frequencies and magnetic fields ($\nu \sim 100 \text{ kHz}$, $H_{app} \leq 200 \text{ Oe}$). Moreover, as the magnetic properties of this class of particles are size-dependent, narrow particle size distributions are critical for an understanding of their magnetic properties and effects on biological cells. With recent advancements in synthetic methods has come the ability to easily prepare a wide range of magnetic NPs that are highly crystalline and uniform in size, granting access to more accurate dynamic studies of surface, finite size effects, and crystal structure contribution in NPs.^{11,12}

For the mentioned applications as well as a fundamental point of view, a considerable effort was focused in ferrite nanocomposites, in particular Fe_3O_4 , MnFe_2O_4 , and CoFe_2O_4 ferrite compounds. For instance, manganese spinel ferrite MnFe_2O_4 NPs can be used as contrast enhancement agents in magnetic resonance imaging technology.¹³ Cobalt ferrite CoFe_2O_4 holds promise in the production of isotropic permanent magnets, magnetic recording, and fluids because it has a very high cubic magnetocrystalline anisotropy, accompanied with a reasonable saturation magnetization value M_s .^{6,14} CoFe_2O_4 has a relatively large magnetic hysteresis in comparison with the rest of the spinel ferrites. Ferrimagnetic particles, such as magnetite (Fe_3O_4), may be applied in ferrofluids for hyperthermia applications. It is currently the only FDA-approved metal oxide nanoparticle.^{15,16}

In spite the fact that “particle-size-effects” in ferrite nanostructure materials have been investigated exhaustively by many authors,^{9,14,16-19} it is interesting to remark that a complete study on ferrite NPs of the same size, shape, and

^{a)} Electronic mail: LSpinu@uno.edu.

crystalline properties but different chemical compositions is still lacking. In particular, the magnetic properties of the ferrite compounds mentioned above are strictly related with their intrinsic effective magnetocrystalline anisotropies, and in such case, the chemical composition of the transition-metal ferrites nanocomposites is an alternative approach to control the magnetic properties of NPs with exactly the same morphological and crystalline features. Therefore, the study of the correlation between these ferrite nanocomposites in the so-called model samples, and at the same time with similar morphological and crystalline properties, is still of growing interest from both a theoretical and technological point of view.

In this paper, we report on the fabrication and thermal relaxation process of model Fe_3O_4 , MnFe_2O_4 , and CoFe_2O_4 ferrite monodomain NPs with sizes near to 10 nm, while concurrently exploring an alternative approach for tuning the dynamic properties of magnetic NPs. In order to meet the demand for both fundamental research and industry applications, the developed process described in this work fulfills the requirements of low-cost and large-scale synthesis of high-quality ferrite NPs. Moreover, the metallic precursors used in this new synthesis are commercially readily available and less toxic than the pentacarbonyl-based compounds, a common precursor used in thermal decomposition reaction. Static and dynamic magnetic experiments by *dc*-, *ac*-magnetometry, and ferromagnetic resonance were conducted with the aim to map and evaluate the thermal relaxation and energy loss of ferrite NPs.

II. EXPERIMENTAL

The inverse spinel ferrite NPs were synthesized using a modified high temperature thermal decomposition method published elsewhere.²⁰ In a typical synthesis, 1 mmol of $\text{Fe}(\text{ac})_2$, 0.5 mmol transition metal acetate $\text{M}(\text{ac})_2$ ($\text{M} = \text{Mn}, \text{Fe}, \text{Co}$), and 6 mmol of oleic acid were added to 15 ml benzyl ether in a three-neck round flask and stirred vigorously. To promote the dissolution of the acetate salts and eliminate the hydrating water molecules the initial solution was heated rapidly to 150 °C and maintained at this temperature for 15 min. The temperature was subsequently increased to 275 °C. After 30 min, the reaction was stopped by removing the heat source and allowing the solution to cool down naturally to room temperature. The resulting powders were recovered from the solution by magnetic separation and washed several times with ethanol and acetone, then separated again and extracted in hexane. For the complete removal of the excess benzyl ether, this purification protocol was repeated three times. Oleic acid-capped magnetic nanocrystals were isolated and then dispersed in various non-polar solvents (chloroform, hexane, etc.) yielding clear, brown colloids which are stable for months against aggregation at room temperature.

The crystal structure, particle size, and distribution of ferrite NPs were analyzed by using a $\text{Cu-}k_\alpha$ X-ray powder Rigaku diffractometer (XRD, $\lambda = 1.5418 \text{ \AA}$) and a JEOL JEM 2010 transmission electron microscope (TEM) at 200 KV.

The *dc*-magnetic properties were measured using a commercial superconducting quantum interference device (SQUID) magnetometer in a temperature range of $T = 4 \text{ K} - 300 \text{ K}$ and field strength up to $H \pm 70 \text{ kOe}$, in the typical experimental measuring-time of $\tau = 100 \text{ s}$.¹ The complex magnetic susceptibility $\chi = \chi' + j\chi''$ of the magnetic NPs was measured as a function of temperature from 4 to 300 K for frequencies ranging from $\nu = 10 \text{ Hz}$ to 10 kHz in a quantum design physical property measurement system (PPMS).

III. RESULTS AND DISCUSSION

Figure 1(a) shows the XRD patterns for the Fe_3O_4 , MnFe_2O_4 , and CoFe_2O_4 powder samples. The peaks are broader due to the smaller sized nanocrystals and the peak positions are centered on the bulk crystal lines with no other features (cubic inverse spinel, $*\text{Fd}3\text{m}$). The presence of Fe_3O_4 in the sample instead of $\gamma\text{-Fe}_2\text{O}_3$ was probed experimentally by using Raman spectroscopy (results not shown) and furthermore confirmed by oxidation experiments at different temperatures. It is well known that Fe_3O_4 can be oxidized to $\gamma\text{-Fe}_2\text{O}_3$ at 250 °C and the resulting gamma oxide be converted into $\alpha\text{-Fe}_2\text{O}_3$ upon oxidation under Ar, similar to the scheme proposed by Sun and co-workers.²¹ More information about the chemical and structural characterization of the ferrite nanoparticles presented in our study can be found in a previous report by Caruntu and co-workers.²² Taking the full width at half-maximum (FWHM) of the most intense peak and using the Scherrer equation,²³ the average crystalline size for the three samples was determined to be around 70% of the TEM histogram mean size (see values in Table I). The scheme in Fig. 1(b) shows the chemical formula and the ideal case of an inverse spinel CoFe_2O_4 , where the Co cation occupies one-half of the octahedral coordination sites. Half of the Fe^{3+} cations occupy the other half of the octahedral coordination sites as well as all of the tetrahedral coordination sites. Figure 2 corresponds to the TEM images and histograms of Fe_3O_4 , MnFe_2O_4 , and CoFe_2O_4 NPs. The

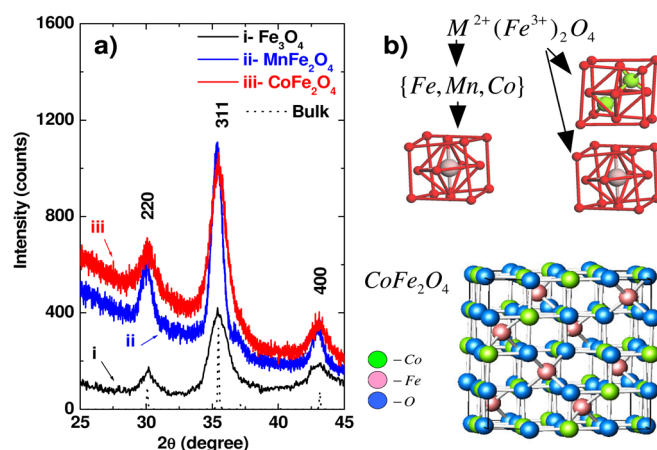


FIG. 1. (Color online) (a) X-ray diffraction patterns of i- Fe_3O_4 , ii- MnFe_2O_4 , and iii- CoFe_2O_4 ferrite nanoparticle samples. The dotted line corresponds to the bulk ferrite. (b) Scheme of the crystalline structure for ideal inverse spinel ferrite composites, where the tetragonal and octahedral sites for the Fe, Mn, and Co ions are depicted.

TABLE I. Structural and magnetic properties. The errors are indicated in brackets.

Sample	Structural		<i>dc</i> -Parameters			<i>ac</i> -Parameters		
	D_{TEM} (nm)	D_{XRD} (nm)	T_B (K)	n/ν (μ_B)	M_S (emu/g) ^a	E_B (K)	K (erg/cm ³)	SLP (erg/s ² *g) ^b
Fe ₃ O ₄	6.9 (0.8)	4.2	29	43.4	83.7 (8.3)	1124	9.01 (11) $\times 10^5$	20
MnFe ₂ O ₄	9.5 (0.9)	7.6	50	40.4	78.0 (8.1)	1600	4.91 (50) $\times 10^5$	217
CoFe ₂ O ₄	8.0 (1.5)	5.3	130	35.4	68.3 (7.0)	4917	25.31 (40) $\times 10^5$	132

^aBulk saturation magnetization values of Fe₃O₄ (92 emu/g), MnFe₂O₄ (80 emu/g), and CoFe₂O₄ (75 emu/g) (Ref. 26).

^bThese values correspond to the maximum of the SLP at $\nu = 10$ KHz, at the temperatures of $T = 43.5$ K (Fe₃O₄), 65 K (MnFe₂O₄), and 217 K (CoFe₂O₄).

histograms of particle size distribution were built by counting 200 particles for each sample, and were fitted with a Gaussian function, $f(D) \propto e^{-\frac{(D-\bar{D})^2}{2\sigma^2}}$, where \bar{D} is the center peak position and σ is the linewidth of the distribution. From the TEM histograms (Fig. 2-right side), the mean particle sizes were determined with the values of 8.0 ± 1.5 nm (CoFe₂O₄ NP), 9.5 ± 0.9 nm (MnFe₂O₄ NP), and 6.9 ± 0.8 nm (Fe₃O₄ NP), showing a clearly high-quality crystalline order with homogeneous cubic-faceted shape. Supporting

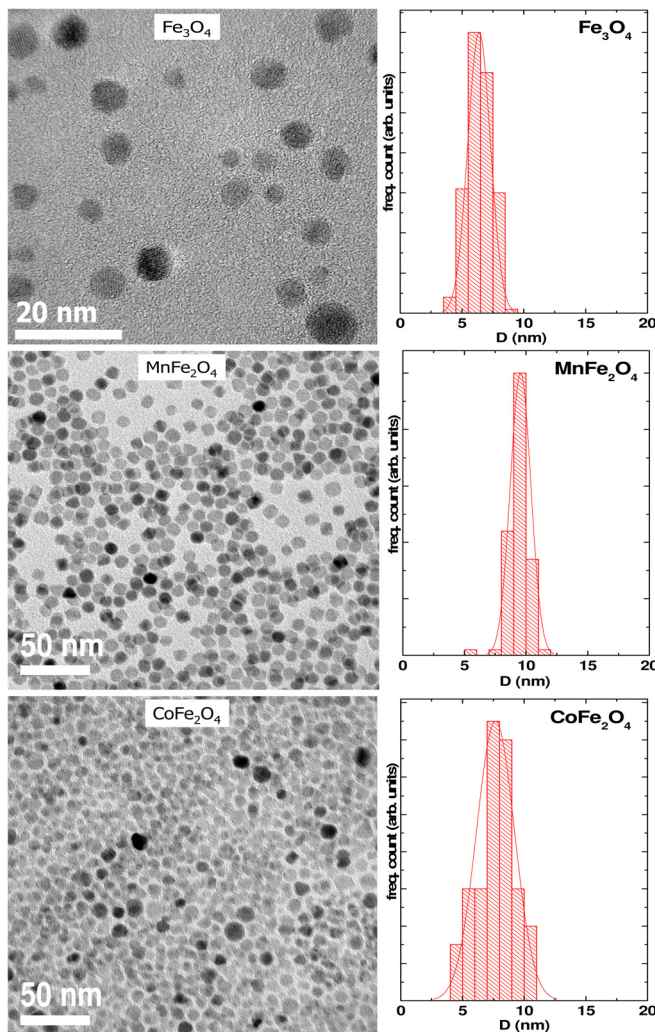


FIG. 2. (Color online) TEM images of Fe₃O₄, MnFe₂O₄, and CoFe₂O₄ ferrite nanoparticles, showing the histograms with narrow size distribution and homogeneous shape of nanoparticles. The continuous red line is the Gaussian fit.

the good chemical, morphological and crystalline homogeneity of these samples, the T -dependence of the dc -magnetic susceptibility under zero-field-cooling and field-cooling conditions (with applied magnetic field of $H = 20$ Oe), are plotted in Fig. 3 ($\chi_{dc} = \frac{M}{H}$). Due to the organic capping protection to avoid the direct contact between particles, the dipole-dipole is the principal mechanism of interaction between them. In the case of Fe₃O₄ NPs, two characteristics can be remarked: (i) the narrow single peak of the M_{ZFC} and (ii) the monotonic increment of the M_{FC} as the temperature drops. Both characteristics are the fingerprints of model monodispersed single magnetic domain NPs with random easy magnetization axis orientations and moderate dipolar interaction.²⁴ The case of the Mn- and Co-ferrite clearly show the enhancement of the magnetocrystalline anisotropy, with intermediate and larger broadening of the M_{ZFC} , respectively. Moreover, in both cases the T -dependence of the M_{FC} show different trends that can be explained through the interplay between the effective anisotropy and magnetic moment per particle (the M_{ZFC-FC} curves for the Co-ferrite NPs are amplified 7 times for a more clear comparison). Table I summarizes the blocking temperature (T_B) for each sample.²⁵ Fig. 4(a) shows the magnetization loops measured at $T = 4$ K and 300 K for the Fe₃O₄, MnFe₂O₄, and CoFe₂O₄ powder samples, respectively. In good agreement with the T -dependence of M_{ZFC-FC} , the magnetization loops at $T = 4$ K correspond to the case of soft (Fe₃O₄), intermediate (MnFe₂O₄), and hard (CoFe₂O₄) single domain anisotropic materials. The three samples do not show any hysteresis at room temperature, as it is evidenced from the magnetization curves.

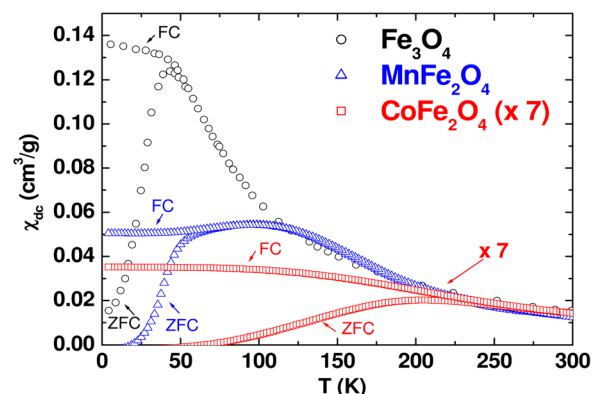


FIG. 3. (Color online) Magnetic susceptibility (χ_{dc}) against- T measured in ZFC and FC modes ($H = 20$ Oe), for the Fe₃O₄, MnFe₂O₄, and CoFe₂O₄ powder samples. The M_{ZFC-FC} curves for the co-ferrite NPs are amplified 7 times for a more clear comparison.

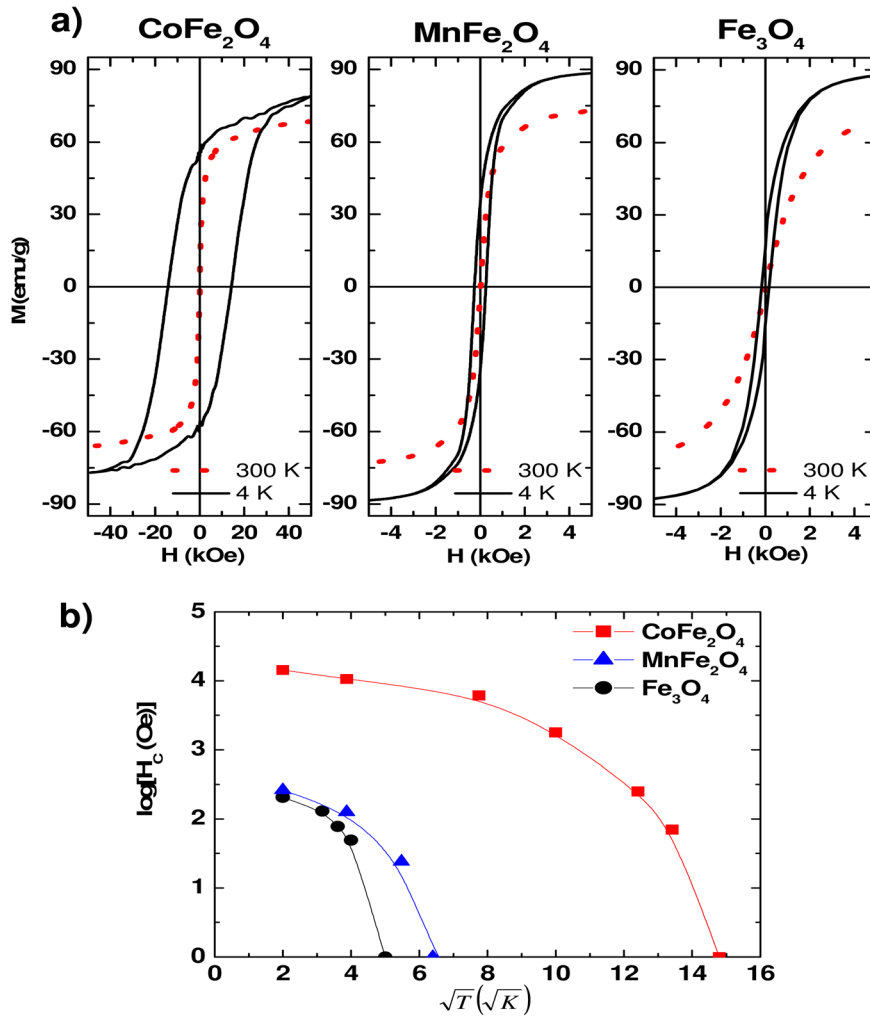


FIG. 4. (Color online) (a) Magnetization loops measured at $T = 4\text{ K}$ and 300 K and (b) coercive field against $-\sqrt{T}$ for the Fe_3O_4 , MnFe_2O_4 and CoFe_2O_4 powder samples. Due to the different strength of the magnetocrystalline anisotropy, the H_c values are plotted in a natural logarithm.

Moreover, for the three samples, different magnetization upper-convex shapes are clearly evidenced; this can be directly related with different effective magnetic moments. Taking into account, the Stoner-Wohlfarth model for homogeneous single magnetic domains and using the Langevin function,¹ $L(x) = \coth(x) - 1/x$ (where $x = n\mu_B H/k_B T$, k_B is the Boltzmann constant and μ_B is the Bohr magneton), the effective magnetic moment per volume was estimated for each sample. Under this condition, the approximate value of $\frac{\mu}{V} \sim 40\mu_B/\text{nm}^3$ is obtained for the three samples ($\bar{V} = \frac{\pi}{6}\bar{D}^3$) sparing these values with the respective bulk ones, the differences are less than 10% for the three samples (see parameters in Table I). For the three samples, the full T -dependence of the coercive fields, H_c , are shown in Fig. 4(b), in good agreement with the Stoner-Wohlfarth $\sqrt{T} - \text{law}$.¹ The magnetic susceptibility against- T with different field amplitudes ($H = 3, 5,$ and 10 Oe) and frequencies ($\nu = 10\text{ Hz}, 100\text{ Hz}, 500\text{ Hz}, 1000\text{ Hz}, 2000\text{ Hz}, 5000\text{ Hz}, 10\text{ kHz}$) was carried out for the characterization of the dynamic response of the ferrite NPs. Since the actual response of the sample to an applied ac -field is measured, the magnetodynamics can be studied through the complex susceptibility ($\chi' + j\chi''$). The real component χ' represents the component of the susceptibility that is in phase with the applied ac -field, while χ'' represents the component that is out of phase. The imaginary

component χ'' is related to the energy losses, or in other words, the energy absorbed by the sample from the ac field. Figure 5(a) shows T -dependence of the real and imaginary component of the susceptibility with an applied ac field of $H_{ac} = 5\text{ Oe}$ ($4\text{ K} \leq T \leq 300\text{ K}$). Similar trends were observed for H_{ac} strengths of 3 Oe and 10 Oe (figure not shown). The χ' versus T shows a single peak for each sample, where a peak-shift to high- T and the drop of the intensity is observed as the frequency increases from $\nu = 10\text{ Hz}$ to 10 kHz . This effect is directly related with the frequency dependence of the blocking temperature of the superparamagnetic NPs as the samples are cooled down.¹ Comparing the χ' versus T components for the Fe_3O_4 , MnFe_2O_4 , and CoFe_2O_4 powder samples, the peaks as function of frequency are located at different ranges of temperature, where this fact is directly correlated with the strength value of the magnetocrystalline anisotropy.¹ Fig. 6 shows the variation of the T_B in the plot of $\ln(\tau/\tau_0)$ versus $1/T_B$ for the three samples ($\tau_0 = 10^{-10}\text{ s}$), where the linear fit corresponding to the Néel law dependence is $\ln\left(\frac{\tau}{\tau_0}\right) = \frac{E_B}{k_B T}$, where E_B is the energy barrier of the NPs. In a first approach, $E_B = K\bar{V}$, where K is the effective anisotropy constant. Therefore, the values of E_B and K were calculated from these experimental results where the larger, intermediate, and lower E_B values were obtained for the Co-, Mn-, and Fe-ferrite NPs, respectively (see values in Table I).

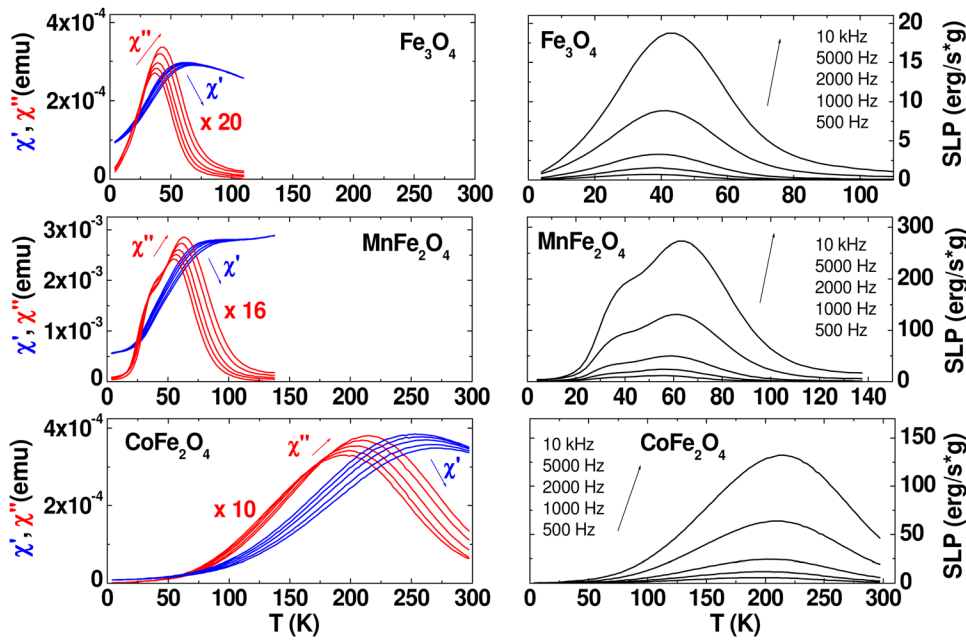


FIG. 5. (Color online) (a) Real (χ') and imaginary (χ'') components of the AC-susceptibility against- T ($H = 5$ Oe). The arrows denote the shift of the peak-position as the frequency rise. (b) SLP for the three ferrite powder samples, where the arrows denote the shift of the peak-position as the frequency rise.

The obtained effective K values are in good agreement with the expected values of Fe₃O₄ (hard 2.0×10^6 erg/cm³-soft 2.1×10^5 erg/cm³), MnFe₂O₄ (8.5×10^4 erg/cm³), and CoFe₂O₄ (between 2.5×10^6 erg/cm³ and 19×10^6 erg/cm³).^{28–30} Consistent with the χ' versus T data, χ'' versus T shows a single peak for each sample, where a shift-peak to high- T and the rise of the intensity are observed as the frequency is increased from $\nu = 10$ Hz to 10 kHz. This effect is directly related with the frequency dependence of the blocking temperature and the enhancement of the energy lost as the frequency rise, where the SLP may be expressed by the imaginary part of the susceptibility, χ'' (Refs. 11 and 12)

$$SLP(H, \nu) = \pi \chi''(\nu) H^2 \frac{\nu}{\rho}, \quad (1)$$

where ρ is the mass density. This formula is restricted to small amplitudes of the magnetic field since the typical

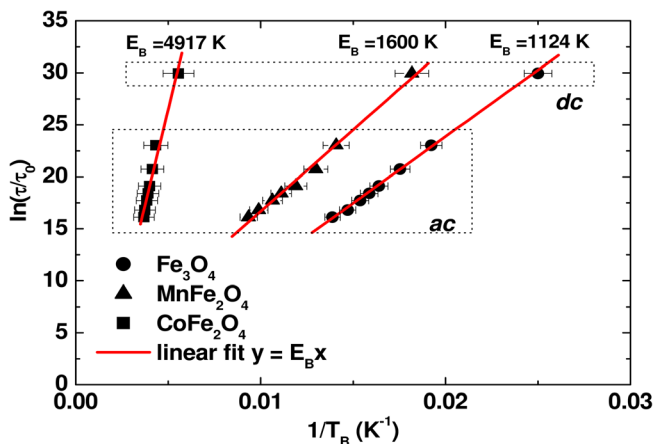


FIG. 6. (Color online) Variation of the T_B in the plot of $\ln(\tau/\tau_0)$ versus $1/T_B$ for the three ferrite samples ($\tau_0 = 10^{-10}$ s). Using the Boltzmann constant, the E_B is given in Kelvin units. The two rectangular blocks in dotted lines are regarding to the experimental points extracted from dc -magnetization (blocking temperature from the M versus T in ZFC and FC conditions) and ac -susceptibility (maximum of the χ' versus T at different frequencies).

magnetic saturation is not comprised. Using the experimental results of χ'' and Eq. (1), Fig. 5(b) shows the SLP results for the three samples. In particular, comparing the three samples at $\nu = 10$ kHz, the MnFe₂O₄ exhibit the maximum of SLP with the value of 273 erg/s·g at $T = 65$ K, whereas for the CoFe₂O₄, a maximum of 132 erg/s·g ($T = 217$ K) was determined (the values are summarized in Table I). A considerable drop in the SLP was determined for the Fe₃O₄, with the value of 20 erg/g·s at $T = 43.5$ K. A remarkable result is the fact that Co-ferrite NPs still shows an energy absorption at room temperature at low frequency and field strength amplitude.

IV. CONCLUSIONS

In conclusion, monodisperse ferrite NPs of Fe₃O₄, MnFe₂O₄, and CoFe₂O₄ with sizes near to 10 nm were synthesized by an organometallic route, and show homogeneous chemical, morphological, and crystalline characteristics. Based on the Stoner-Wohlfarth model for homogeneous single magnetic domains NPs and Néel relaxation process, the thermal relaxation process through static and dynamic magnetic measurements was analyzed. Due to the intrinsic chemical characteristics and magnetocrystalline anisotropy of the Fe-, Mn-, and Co-ferrite NPs with similar size, the energy barrier can be tuned in a large spectrum with values ranging between $1100 \text{ K} \leq E_B \leq 7300 \text{ K}$, showing an alternative path for tuning the magnetic dynamic response. This is in contrast to the well-known mechanism that occurs through a particle-size-effect. With similar particle size, high crystalline quality (higher than 70% respect to the full particle size) and homogeneous shape, the magnetic correlation between these samples were determined by static and dynamic means. The specific loss power efficiencies were evaluated for the three ferrite samples. In spite of some recent publications, such as Bae *et al.*,²⁷ the promising results presented in this paper show that ferrite nanoparticles can be useful for

hyperthermia experiments in the frequency range below 100 kHz and low applied magnetic field ≤ 200 Oe. Comparing the three samples at the maximum *ac* frequency, $\nu = 10$ kHz, MnFe_2O_4 exhibits the maximum efficiency with a value of $273 \text{ erg/s} \cdot \text{g}$ at $T = 65$ K; whereas, CoFe_2O_4 , a maximum of $132 \text{ erg/s} \cdot \text{g}$ ($T = 217$ K) was determined (Table I). A considerable drop in the efficiency was determined for the Fe_3O_4 , with a value of $20 \text{ erg/g} \cdot \text{s}$ at $T = 43.5$ K. The dynamic response and specific form of particle recognition reported in this work will be used for subsequent studies that provides knowledge of the possibly significant presence, identity, and/or quantity of magnetic NPs or energy in the local environment.

ACKNOWLEDGMENTS

J.V. and L.S. thank Dr. John B. Wiley and Mr. Denny Ross Lenormand for prereading the manuscript. This work is supported by the Department of Defense through the DARPA Grant No. HR 0011-09-0047, the National Science Foundation, through the Grant Nos. EPS 1003897 and NSF-DMR-1004869 and the Office of Research and Sponsored Programs (ORSP) at the University of New Orleans. Louisiana Board of Regents Contract #LEQSF(2007-12)-ENH-PKSFI-PRS-04.

- ¹J. L. Dormani, L. Bessaist, and D. Fiorani, *J. Phys. C: Solid State Phys.* **21**, 2015 (1988).
- ²M. Knobel, W. C. Nunes, L. M. Socolovsky, E. De Biasi, J. M. Vargas, and J. C. Denardin, *J. Nanosci. Nanotechnol.* **8**, 2836 (2008); and the references therein.
- ³E. Lima, Jr., J. M. Vargas, R. D. Zysler, H. R. Rechenberg, R. Cohen, J. Arbiol, G. F. Goya, A. Ibarra, and M. R. Ibarra, *Nanotechnology* **20**, 045606 (2009).
- ⁴G. Sheet, A. R. Cunliffe, E. J. Offerman, C. M. Folkman, Chang-Beom Eom, and V. Chandrasekhar, *J. Appl. Phys.* **107**, 104309 (2010).
- ⁵Y. Cedeo-Mattei, O. Perales-Pérez, O. N. C. Uwakweh, and Y. Xin, *J. Appl. Phys.* **107**, 09A741 (2010).
- ⁶Y. Cedeo-Mattei, O. Perales-Pérez, M. S. Tomar, F. Roman, P. M. Voyles, and W. G. Stratton, *J. Appl. Phys.* **103**, 07E512 (2008).
- ⁷S. P. Gubin, Yu A. Koksharov, G. B. Khomutov, and G. Yu Yurkov, *Russ. Chem. Rev.* **74**, 489 (2005).
- ⁸A. H. Latham and M. E. Williams, *Acc. Chem. Res.* **41**, 411 (2008).

- ⁹A. H. Habib, C. L. Ondeck, P. Chaudhary, M. R. Bockstaller, and M. E. McHenry, *J. Appl. Phys.* **103**, 07A307 (2008).
- ¹⁰S. R. Dave, X. Gao, Wiley Interdisciplinary Reviews, www.wiley.com/wires/nanomed (John Wiley & Sons, Inc., 2009), Vol. 1, p. 583.
- ¹¹R. Hergt, S. Dutz, and M. Zeisberger, *Nanotechnology* **21**, 015706 (2010).
- ¹²A. M. Derfus, G. Maltzahn, T. J. Harris, T. Duza, K. S. Vecchio, E. Ruoslahti, and S. N. Bhatia, *Adv. Mater.* **19**, 3932 (2007).
- ¹³D. Kim, D. E. Nikles, and C. S. Brazel, *Materials* **3**, 4051 (2010).
- ¹⁴R. D. Desautels, J. M. Cadogan, and J. van Lierop, *J. Appl. Phys.* **105**, 07B506 (2009).
- ¹⁵N. Singha, G. J. S. Jenkinsa, R. Asadib, and S. H. Doaka, *Nano Rev.* **1**, 5358 (2010).
- ¹⁶O. E. Ayala-Valenzuela, J. A. Matutes-Aquino, J. T. Elizalde Galindo, and C. E. Botez, *J. Appl. Phys.* **105**, 07B524 (2009).
- ¹⁷A. L. Gurgel, J. M. Soares, D. S. Chaves, D. S. Chaves, M. M. Xavier, M. A. Morales, and E. M. Baggio-Saitovitch, *J. Appl. Phys.* **107**, 09A746 (2010).
- ¹⁸Q. Gao, G. Hong, J. Ni, W. Wang, J. Tang, and J. He, *J. Appl. Phys.* **105**, 07A516 (2009).
- ¹⁹K. H. Hsu, J. H. Wu, Y. Y. Huang, L. Y. Wang, H. Y. Lee, and J. G. Lin, *J. Appl. Phys.* **97**, 114322 (2005).
- ²⁰L. D. Tung, V. Kolesnichenko, D. Caruntu, N. H. Chou, C. J. O'Connor, and L. Spinu, *J. Appl. Phys.* **93**, 7486 (2003); C. J. O'Connor, Y. S. L. Buisson, S. Li, S. Banerjee, R. Premchandran, T. Baumgartner, V. T. John, G. L. McPherson, J. A. Akkara, and D. L. Kaplan, *J. Appl. Phys.* **81**, 4741 (1997).
- ²¹S. Sun, H. Zeng, D. B. Robinson, S. Raoux, P. M. Rice, S. X. Wang, and G. Li, *J. Am. Chem. Soc.* **126**, 273 (2004).
- ²²S. Adireddy, C. Lin, V. Palshin, Y. Dong, R. Cole, and Gabriel Caruntu, *J. Phys. Chem. C* **113**, 20800 (2009).
- ²³R. M. Cornell and U. Schwertmann, *The Iron Oxides: Structure, Properties, Reactions, Occurrence and Uses* (VCH: New York, 1996); C. B. Murray, C. R. Kagan, and M. G. Bawendi, *Annu. Rev. Mater. Sci.* **30**, 545 (2000).
- ²⁴J. M. Vargas, W. C. Nunes, L. M. Socolovsky, M. Knobel, and D. Zanchet, *Phys. Rev. B* **72**, 184428 (2005).
- ²⁵The point where the M_{ZFC} and M_{FC} curves join each other is defined as the irreversible temperature, T_{irr} . The blocking temperature is calculated by the equation, $d(M_{ZFC}-M_{FC})/dT \propto T f(T)$, details in Ref. [J. M. Vargas, J. Gómez, R. D. Zysler, and A. Butera, *Nanotechnology* **18**, 115714 (2007)].
- ²⁶H. Lu, W. T. Zheng, and Q. Jiang, *J. Phys. D: Appl. Phys.* **40**, 320 (2007).
- ²⁷M. Jeun, S. J. Moon, H. Kobayashi, H. Y. Shin, A. Tomitaka, Y. J. Kim, Y. Takemura, S. H. Paek, K. H. Park, Kyung-Won Chung, and S. Bae, *Appl. Phys. Lett.* **96**, 202511 (2010).
- ²⁸S. Yoon and K. M. Krishnan, *J. Appl. Phys.* **109**, 07B534 (2011)
- ²⁹T. E. Torres, A. G. Roca, M. P. Morales, A. Ibarra, C. Marquina, M. R. Ibarra, and G. F. Goya, *J. Phys.: Conf. Ser.* **200**, 072101 (2010).
- ³⁰E. Lima, Jr., A. L. Brandl, A. D. Arelaro, and G. F. Goya, *J. Appl. Phys.* **99**, 083908 (2006).